STUDY AND EXPERIMENT ON A CORN FLEXIBLE THRESHING TECHNOLOGY WITH SINGLE-POINT HINGED STRUCTURE BASED ON DEM-MBD COUPLING

/

基于 DEM-MBD 耦合的单点铰接玉米柔性脱粒技术研究与试验

Qiming YU[1)], Jianning YIN[1)], Yipeng CUI[1)], Zehao ZHA[1)], Pengxuan GUAN[1)], Yang WANG[1)], Xinxin WANG[1)], Duanyang GENG[1*)]

[1)] School of Agricultural Engineering and Food Science, Shandong University of Technology, Zibo 255000, China

** Corresponding authors. Tel.: +86 13668641238; E-mail address: dygxt@sdut.edu.cn (D.Y. Geng)*

DOI: https://doi.org/10.35633/inmateh-76-100

Keywords: *DEM-MBD coupled simulation; corn; flexible threshing; kernel breakage rate; threshing device*

ABSTRACT

To address the issues of high kernel breakage rate and poor adaptability in threshing devices for direct corn kernel harvesting, this study proposes a flexible threshing device based on a single-point hinged structure. In this design, the threshing elements are flexibly mounted via single–point hinges, allowing them to rotate upon impacting corn kernels. This rotational motion provides an impact-buffering effect during the threshing process, thereby reducing the risk of kernel breakage. By comparing the dynamic characteristics of the single-point hinged flexible structure with those of a rigid structure, the superiority of the proposed device is confirmed. A contact force model is established to analyze key parameters influencing threshing performance, identifying the mass of the threshing element, rotational speed, and structural configuration as the primary factors. A coupled simulation model was developed using RecurDyn and EDEM software to investigate the effects of threshing element mass, rotational speed, and structural configuration on the kernel breakage rate and unthreshed grain rate of the device, and to determine the optimal parameter range. Based on a three-factor, three-level orthogonal experimental design, the optimal working parameters of the device were identified as follows: threshing element mass of 200 g, rotational speed of 600 r/min, and a composite structural configuration. Under these conditions, the kernel breakage rate was 3.95% and the unthreshed grain rate was 0.88%, meeting the practical requirements for harvesting performance. This study provides theoretical support and a technical pathway for the design of high-efficiency, low-damage threshing devices for direct corn kernel harvesting.

摘 要

为解决玉米籽粒直收中脱粒装置对籽粒破碎率高、柔性适应性差等问题，本文提出了一种基于单点铰接结构的玉米柔性脱粒装置。该装置通过将脱粒元件以单点铰接的形式柔性安装，让脱粒元件在冲击玉米籽粒的同时可以回转，旋转脱粒过程具有缓冲冲击能力，以降低籽粒破碎风险。通过将单点铰接柔性结构与刚性结构脱粒时的动力学特性进行对比，确定该装置的优越性。建立接触力模型并分析影响脱粒效果的关键参数，确定了脱粒元件质量、转速和结构形式作为主要影响因素。基于 RecurDyn 和 EDEM 软件构建了耦合仿真模型，探究了该装置中脱粒元件的质量、转速以及结构形式对籽粒破碎率和未脱净率的影响规律，并确定了较优参数区间。通过三因素三水平正交试验，确定了该装置的最佳工作参数为：脱粒元件质量为 200g、转速为 600 r/min、结构形式为组合型，此时籽粒破碎率为 3.95%，未脱净率为 0.88%，作业性能满足了实际收获需求。本研究为高效、低损伤的玉米籽粒直收脱粒装置设计提供了理论支持和技术路径。

INTRODUCTION

Direct corn kernel harvesting has emerged as a major developmental trend in China's corn production due to its advantages such as high operational efficiency, reduced mechanical losses, and decreased dependence on post-harvest drying and manual labor *(Jun et al., 2018, Mircea et al., 2020, Nenciu et al., 2021)*. This method has been widely promoted across key corn-producing regions, including Northeast China and the Huang–Huai–Hai Plain *(Meizhou et al., 2020, Qing et al., 2024)*. However, due to the relatively high moisture content of corn at harvest, the performance requirements for the threshing device in kernel–direct harvesting systems have become more stringent-particularly in achieving a high threshing rate while effectively controlling the kernel breakage rate. To reduce kernel breakage, many researchers in China have proposed flexible threshing technologies.

For example, a bionic flexible threshing technology was developed, inspired by the biomechanics of the human thumb, which significantly reduces kernel damage while maintaining a high threshing rate *(Jiale et al., 2023)*. Similarly, a flexible resin hammer-claw threshing system was developed, achieving low-damage threshing for corn *(Zhanbin et al., 2020)*. A novel composite threshing device incorporating flexible teeth and dual-torsion-spring short rasp bars was designed, enabling segmented flexible threshing that further reduces kernel breakage *(Meizhou et al., 2020)*. Clearly, flexible threshing has proven effective in reducing kernel damage. However, challenges such as component fatigue and wear have limited its large-scale application *(Lin et al., 2024; Vlăduț et al., 2022; Vlăduț et al., 2023)*. To address this, the present study proposes a flexible threshing technology in which the threshing element is hinged to the threshing rod. A mechanical model of the contact force between the flexible threshing element and corn kernels is established to identify key parameters. Using a DEM–MBD coupled simulation, the effects of different threshing element masses, rotational speeds, and structural configurations on the contact performance with corn ears are investigated. Furthermore, bench-scale experiments are conducted to determine the optimal parameters. This study provides theoretical support for the development of high-efficiency, low-damage corn kernel direct harvesting technologies.

MATERIALS AND METHODS

Overall structure and working principle

As shown in Figure 1, the single-point hinged flexible corn threshing device mainly consists of threshing elements, a drive shaft, upper cover, perforated screen, torque sensor, feed inlet, V–belt transmission system, gearbox, frame, and motor. During the threshing process, corn ears are fed through the feed inlet. The motor drives the drive shaft via the V–belt, which in turn rotates the threshing elements. Under the repeated action of the rotating threshing elements, the kernels are separated from the cob. The detached corn kernels pass through the perforated screen, achieving separation from the cob, while the cob is discharged from the machine by the continuous action of the helically arranged threshing elements. During this process, when the high-speed rotating threshing element strikes a corn kernel, it undergoes reverse rotation around the hinge axis due to resistance from the corn ear, as illustrated in Figure 2. This reverse rotation acts as a buffer against the impact load on the kernel, thereby reducing kernel damage. The structural parameters of the threshing test bench are shown in Table 1.

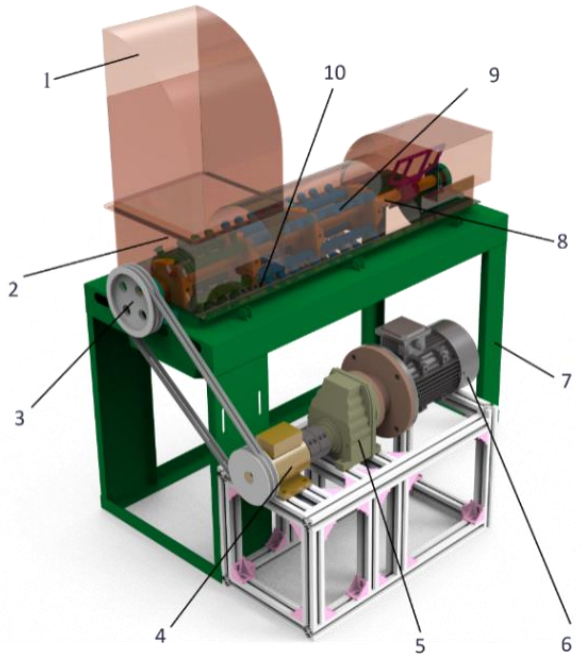

Fig. 1 - Schematic structure of the single-point hinged flexible corn threshing test bench
1 - Feeding inlet; 2 - Upper cover plate; 3 - V-belt drive system; 4 - Torque sensor; 5 - Reducer; 6 - Motor; 7 - Rack; 8 - Drive shaft; 9 - Threshing element; 10 - Hole punching sieve

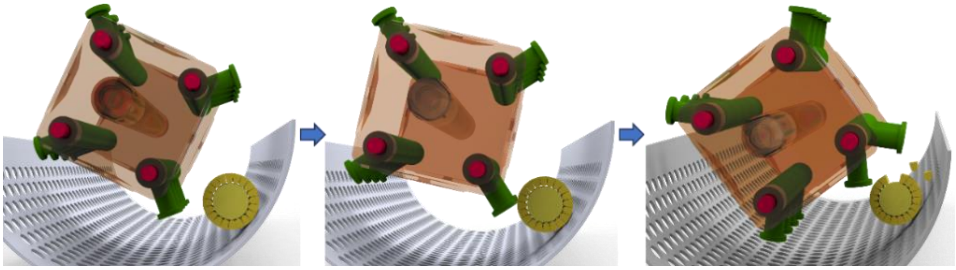

Fig. 2 - Schematic diagram of the threshing process of the single-point hinged flexible device

Table 1

Structural Parameters of the Threshing Test Bench

Parameter	Value
Dimensions (L × W × H) (mm)	1200 × 510 × 1400
Rotational speed of threshing drum (r/min)	0–1000
Threshing clearance (mm)	40
Feeding rate (kg/s)	2

Threshing Load Analysis of Corn Ears in a Single-Point Hinged Structure

To determine the threshing load exerted on the corn ear during the flexible threshing process, a comparative analysis was conducted between the load–bearing conditions rigid (where the threshing element is rigidly fixed to the connecting shaft) and flexible threshing configurations *(Kiniulis et al., 2018)*. As shown in Figure 3(a), the threshing element is in a critical pre-collision state, about to impact the corn ear. At this moment, the motion states of both the rigid and single-point hinged flexible threshing elements are essentially the same. Figure 3(b) illustrates the scenario in which the rigid threshing element comes into contact with the corn ear. In this case, F represents the contact force on the corn ear, directed tangentially to the circular motion of the threshing element; $\mathrm{F_N}$ is the supporting force from the concave screen; mg denotes the gravitational force of the corn ear; and f is the frictional force from the concave screen acting on the ear. During rigid threshing, the threshing element is fixed and non-flexible, directly exerting an impact force on the corn ear. This impact is transmitted rapidly and in a concentrated manner over a relatively long duration, often resulting in strong localized pressure on the corn ear and causing kernel breakage *(Duane et al., 1972)*. In contrast, Figure 3(c) shows the flexible threshing process. When the threshing element strikes the corn ear, it undergoes reverse buffering due to its ability to rotate about the hinge axis. This prevents continuous compression of the corn ear, significantly reducing the threshing load applied by the element and minimizing kernel damage.

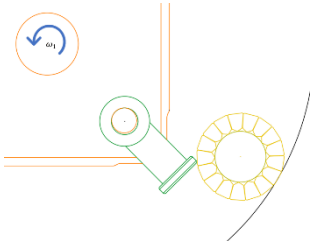

(a) critical moment before collision

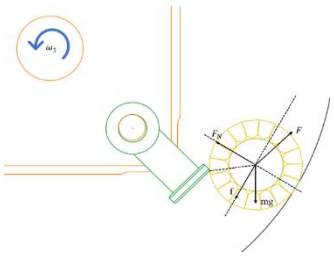

(b) Mechanical Analysis of the Contact Process in Rigid Threshing

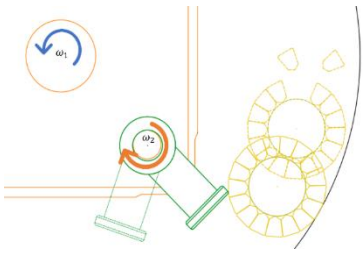

(c) Mechanical Analysis of the Contact Process in Single-Point Hinged Flexible Threshing

Fig. 3 - Comparison of Contact Mechanics: Single-Point Hinged Flexible vs. Rigid Threshing

Contact Force Analysis

In the threshing process, the separation of kernels from the cob depends on the impact load applied by the threshing component to the corn kernels. It is evident that the greater the applied force, the more favorable the separation of kernels from the cob becomes. However, an excessive force may lead to an increased kernel breakage rate *(Yajun et al., 2021)*. Conversely, if the applied force is too small, it may result in a higher unthreshed rate. Therefore, it is necessary to analyze the impact load exerted by the threshing component on the corn ear. Based on the threshing process of the device (Figure 3), the following assumptions are made *(Zhenjie et al., 2021)*:

（1）Initial velocity of corn ear v_c=0.

（2）There is no friction between the threshing element and the corn kernel.

（3）At the critical moment before the collision, the threshing element and the maize are considered as a system, ignoring the influence of other components.

Momentum change of the threshing element before and after the collision Δp_h:

$$\Delta p_h = m_h(v_h' - v_h) \tag{1}$$

In the formula, m_h—Thresher element mass;

v_h—Pre-collision velocity of the threshing element;

v_h'—Post-collision velocity of the threshing element.

Momentum change of the corn before and after the collision Δp_c:

$$\Delta p_c = m_c(v_c' - v_c) \tag{2}$$

In the formula, m_c—Mass of the corn;

v_c—Corn pre-collision velocity;

v_c'—Velocity of the corn after collision.

During the collision process, the total momentum of the system is conserved, and thus we can derive:

$$m_h v_h + m_c v_c = m_h v_h' + m_c v_c' \tag{3}$$

Simplifying:

$$m_h(v_h - v_h') = m_c(v_c' - v_c) \tag{4}$$

The contact force F can be expressed according to the impulse-momentum theorem as:

$$F \cdot t = \Delta p_h$$

In the equation, *t* represents the collision time. It can be concluded that:

$$F = \frac{\Delta p_h}{t} = \frac{m_h(v_h' - v_h)}{t} \tag{5}$$

Assuming the collision is an inelastic collision, the collision coefficient $e(0 \le e \le 1)$ is defined as:

$$e = \frac{v_c' - v_h'}{v_h - v_c} \tag{6}$$

The coefficient of restitution e is defined as:

e=1 represents a perfectly elastic collision, meaning there is no energy loss and kinetic energy is conserved.

e=0 represents a perfectly inelastic collision, where the objects stick together after the collision, resulting in the maximum kinetic energy loss.

0< e <1 represents a partially elastic collision, where some of the kinetic energy is converted into other forms of energy, such as heat or deformation energy.

By combining Equation (4) with Equation (6):

$$v_h' = \frac{(1+e)m_c v_c + (m_h - em_c)v_h}{m_h + m_c} - v_h \tag{7}$$

Substituting Equation (7) into Equation (5), we obtain:

$$F = \frac{m_h}{t}\left[\frac{(1+em_c v_c + (m_h - em_c)v_h}{m_h + m_c} - v_h\right] \tag{8}$$

After simplification:

$$F = \frac{m_h}{t(m_h + m_c)}[(1+e)m_c(v_c - v_h) - em_c v_h] \tag{9}$$

Assuming the initial velocity of the corn ear:

$$F = \frac{m_h m_c (1+e)}{t(m_h+m_c)} v_h \quad (10)$$

The initial velocity of the threshing element v_h can be expressed as:

$$v_h = \frac{2\pi r_h n}{60} \quad (11)$$

where: n –rotational speed of the element;

r_h – the rotational radius of the threshing element.

Substituting Equation (11) into Equation (10), we obtain:

$$F = \frac{m_h m_c (1+e) 2\pi r_h n}{60t(m_h+m_c)} \quad (12)$$

It is evident that, without altering the structural configuration of the threshing element, adjusting the mass m_h and angular velocity ω_h of the threshing element allows for regulation of the impact load, thereby achieving the objective of reducing kernel damage.

Determination of Experimental Factors

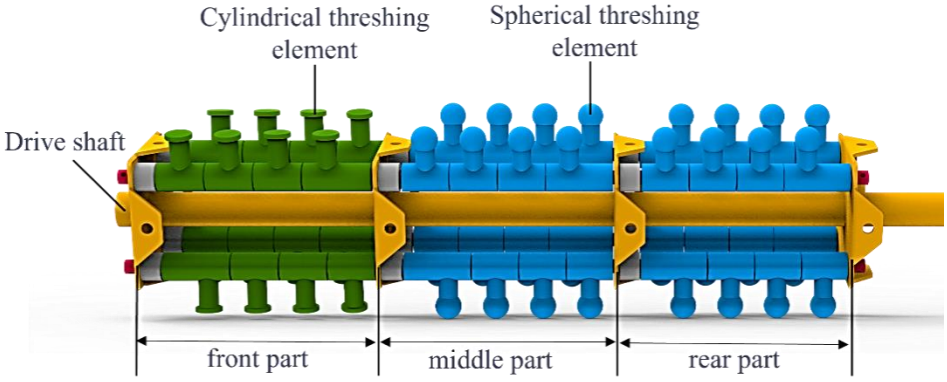

Fig. 4 - Arrangement of Combination-Type Threshing Elements

In this study, the threshing components were fabricated from medium–carbon steel (No. 45 steel), which provides high wear resistance and sufficient structural strength under prolonged operation. To reduce the aggressiveness of the threshing component surface and mitigate kernel damage, the working surfaces were polished to a smooth finish and all edges were chamfered with a rounded radius of 2 mm. These treatments reduce localized stress concentrations upon contact with kernels, thereby lowering the risk of visible cracks or peeling while maintaining the necessary threshing performance. The threshing components are available in two forms: flat–head and ball–head. The flat-head threshing component has a stronger ability to grab and transport the corn ears, which leads to a larger contact force on the corn kernels. On the other hand, the ball-head threshing component has a weaker ability to grab and transport the corn ears, but it is gentler during the threshing process *(Yuan et al., 2021)*. Considering that the impact load is larger when the kernels are not yet detached, and once a kernel is partially separated, the impact load on adjacent kernels decreases significantly, it is necessary to enhance the grabbing and transporting ability in the feeding section. Therefore, the front feeding section uses flat–head threshing components, while the middle and rear sections use ball-head threshing components (as shown in Fig. 4). In comparison to using a single type of threshing component, the combination of different forms in the threshing component theoretically ensures both high threshing efficiency and reduced damage to the corn ears in the middle and rear sections of the threshing zone. To verify the superiority of the combination–type threshing component, both simulation and bench tests were conducted, comparing single-type components with the combined-type components. Based on the analysis in Section “Contact Force Analysis”, the mass and speed of the threshing components are selected as experimental factors. According to the literature, experiments were conducted at rotational speeds of 400 r/min, 500 r/min, 600 r/min, 700 r/min, and 800 r/min *(Xin Ping, 2021)*. At low speeds, the mass must be large enough to ensure that the unthreshed rate meets the requirements. At high speeds, the mass should not be too large to avoid excessive kernel breakage. Preliminary experiments determined that at 400 r/min, a threshing component mass of 260 g meets the unthreshed rate requirement, while at 800 r/min, a mass of 140g meets the breakage rate requirement. Therefore, five mass levels (260 g, 230 g, 200 g, 170 g, and 140 g) were selected for the experiment. First, simulation tests were performed to determine the optimal range, and then, based on bench orthogonal experiments, the optimal parameters were identified.

DEM-MBD COUPLED MODEL AND SIMULATION TEST

Establishment of the DEM Model

To accurately establish a Discrete Element Method (DEM) model of corn, 50 corn ears of the widely cultivated variety "Zhengdan 958" in Shandong Province were selected, and their morphological and structural dimensions were measured, as shown in table 2. Based on the diameter and length of the cob, a coordinate sketch of the corn kernels was created in SolidWorks, and the kernel coordinates were exported using a macro command and then imported into EDEM software to construct a complete corn ear model *(Mousaviraad and Tekeste, 2024; Xiaoyu et al., 2022)*, as shown in Figure 6.

To determine the influence of the flexible threshing device on the contact force acting on the corn ear, the ear model was simplified by replacing the corn kernels with spherical particles. The characteristic parameters of the corn ear and the threshing device materials are shown in Table 3 and Table 4 *(Dandan et al., 2021; Horabik et al., 2017; Zhe et al., 2018)*.

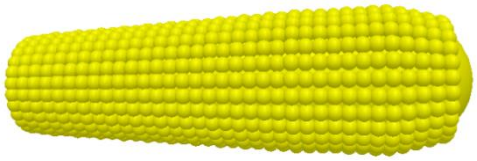

Fig. 5 - Corn Cob Model

Table 2

Dimensions of Corn Ear and Cob Shaft

Item	Corn ear		Maize Cob		Axial Length (mm)
	Large End Diameter (mm)	Small End Diameter (mm)	Large End Diameter (mm)	Small end diameter(mm)	
Maximum	56.47	47.31	36.18	28.78	203
Minimum	45.34	39.68	27.45	21.56	145
Mean	52.35	45.69	31.46	25.47	176
Standard Deviation	2.14	1.87	1.63	1.43	9.44

Table 3

Parameters of materials

Attributes	Ear of Corn	Steel
Poisson ratio	0.4	0.3
shear modulus (MPa)	127	7.9×10^4
Density（kg/m^3）	1197	7850

Table 4

Parameters of mutual materials

Contact Form	Corn–Corn	Corn–Steel
Coefficient of restitution	0.086	0.332
Coefficient of static friction	0.484	0.512
Coefficient of rolling friction	0.103	0.097

DEM-MBD Coupled Model Construction

To expedite the simulation process and minimize the settings for constraint and contact parameters, unnecessary components in the simulation model of the threshing test rig were eliminated. A simplified model of the threshing device, incorporating three different combinations of threshing elements, was developed using SolidWorks and imported into RecurDyn software in STEP format, as shown in Figure 6. Based on the operational process of the single-point hinged maize threshing test rig, constraint and motion conditions between the components were defined in RecurDyn. Using Ground as the reference, fixed constraints were applied to the housing and the perforated screen of the threshing device. Fixed constraints were also established between the connection shaft of the threshing elements and the drive shaft. Rotational constraints were assigned to both the main shaft and the threshing elements, referencing their respective rotational axes.

Additionally, a motion function was applied to the drive shaft's rotational joint using the Motion module to ensure that the drive shaft rotated at a constant speed, as specified. After finalizing the parameter settings in RecurDyn, the simulation model was exported as a wall file format via the External SPI module.

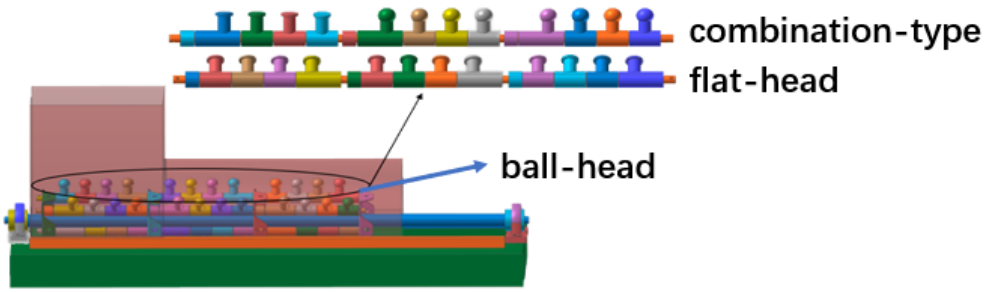

Fig. 6 - MBD Simulation Models of Three Structural Forms

Simulation Experiment

To reflect the differences in the threshing process for different types of threshing elements and to determine the optimal parameter range for rotational speed and threshing element mass for the bench test, coupled simulation experiments were conducted. Based on the analysis in section “Determination of Experimental Factors”**,** the experimental factors chosen were the type of threshing element structure, rotational speed, and the mass of the threshing element. The threshing element structures include cylindrical, spherical, and combined types. Rotational speeds of 400 r/min, 500 r/min, 600 r/min, 700 r/min, and 800 r/min were selected, and the masses of the threshing elements were set at 260 g, 230g, 200 g, 170 g, and 140 g.

During the simulation process, part attributes were set in RecurDyn software, and the user input option was used to set different threshing element masses. The speed of the rotating axis was controlled by adjusting the “motion” module to achieve different rotational speeds. A particle factory was added at the feed inlet, with the feeding rate set to 2 kg/s. The gravitational direction was set to the -Z direction. The total simulation time was set to 6 seconds with a time step of 19.17%, and data was saved every 0.1 seconds. The simulation process is shown in Figure 7.

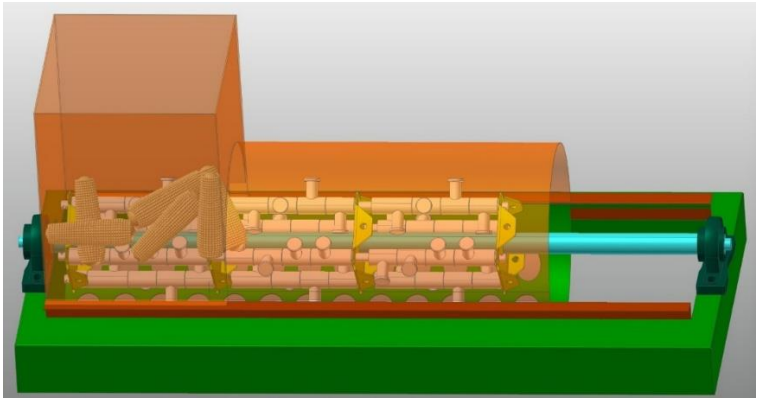

Fig. 7 - Coupled Simulation Model

Bench Test

The single–point hinged corn flexible threshing test stand was used for the bench test, conducted at the experimental field in Hejiayan Tuan Village, Juxian, Rizhao City, Shandong Province (Figure 8a). The threshing device uses a scraper-type conveyor for feeding, with a torque sensor connected at the small pulley to monitor the torque change at the input end of the threshing process in real-time. The cylindrical and spherical threshing components used in the bench test are shown in Figure 8b. The initial mass of the threshing components is 230g, which is reduced to the required mass by drilling holes in the components for the test. The motor speed is controlled by a frequency converter, and a grain collection box is placed at the bottom. The corn variety used in the test is Zheng dan 958, with a moisture content of 28.36%.

According to (GB/T21962-2020) Technical Regulations for Corn Harvesting Machinery and (GB/T5982-2017) Threshing Machine Testing Methods, the test factors include threshing component mass, drum speed, and threshing component structure. Corn ears are fed at a rate of 2 kg/s, and the test evaluation indices are kernel breakage rate and the unthreshed rate. Each test group is repeated three times, and the average value is taken.

The formula for calculating the indices is as follows:

$$Z_s = \frac{W_s}{W_i} \times 100\%$$

Let Z_s denote the kernel damage rate (%), where W_s represents the mass of damaged kernels (g), defined as the total mass of kernels exhibiting visible cracks or peeled surfaces, and W_i is the total mass of kernels in the sample (g).

The threshing performance index is defined as follows:

$$S_w = \frac{W_j}{W_z} \times 100\%$$

where: S_w – threshing completeness rate (%);

W_j – total mass of kernels remaining on the cob (g);

W_z – total mass of all kernels, including both threshed and unthreshed ones (g).

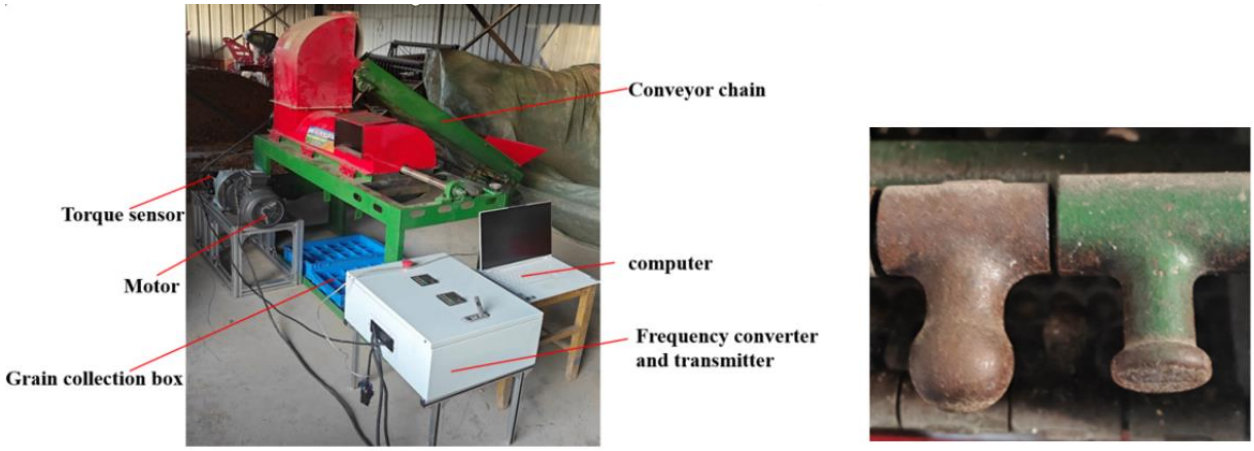

(a) (b)

Fig. 8 - Test Stand for Threshing Device

RESULTS AND DISCUSSION

Analysis of Single-Factor Simulation Results

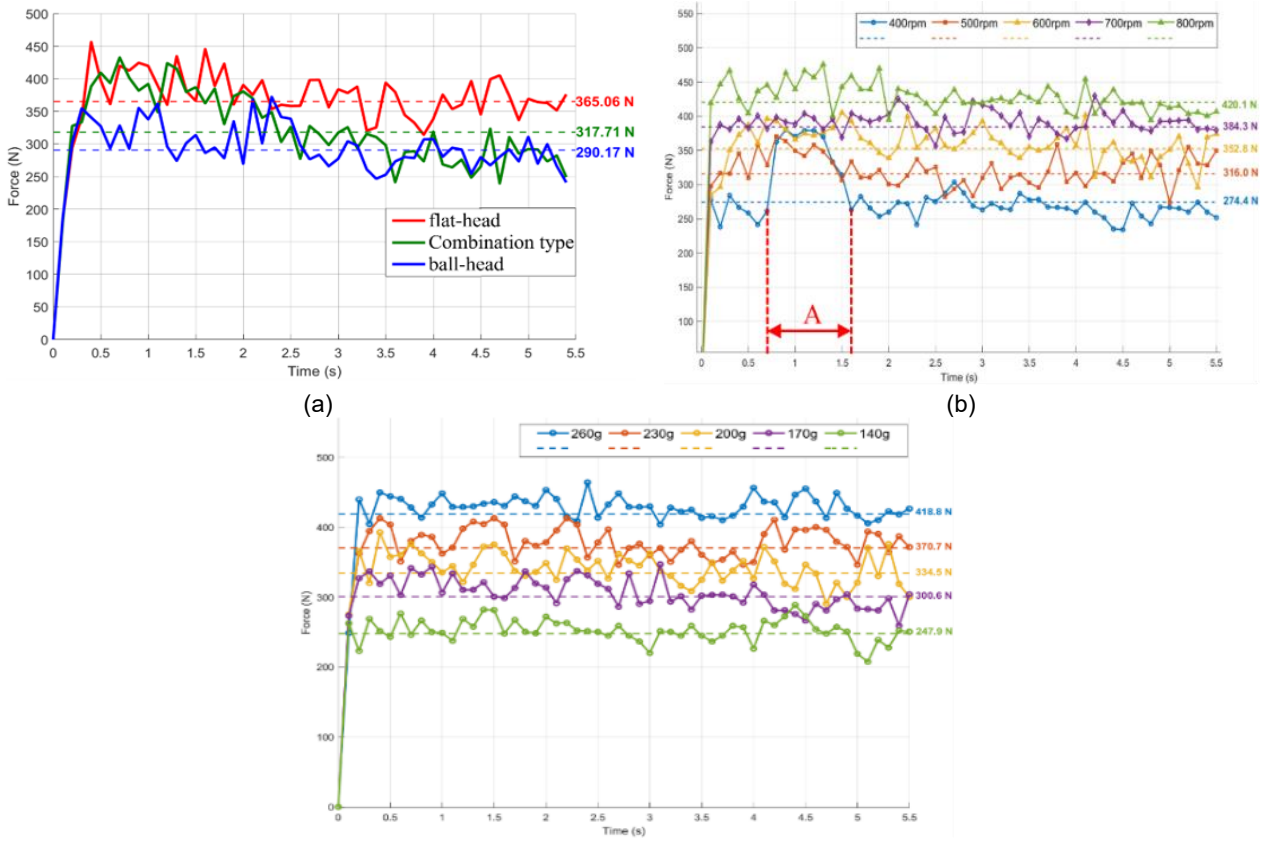

(a) (b)

(c)

Fig. 9 - Simulation Test Results

Figure 9a shows the variation curves of the contact force between different threshing elements and corn ears over time. In terms of overall trends, the flat–head threshing element consistently generates a relatively high contact force throughout the threshing process, with an average value of 365.06 N. In contrast, the ball–head threshing element maintains a lower contact force, averaging 290.17 N. This indicates that under the same conditions, the flat-head element exerts a greater force on the kernels, making kernel damage more likely.

In the combination configuration, flat–head elements are arranged at the front section, while ball–head elements are installed in the middle and rear sections. As a result, before 2.5 s, when the corn ear is in the front section, the contact force is higher; after 2.5 s, as it moves to the middle and rear sections, the contact force decreases. The overall average contact force in this configuration is 317.71 N. The simulation results align with expectations: the combination setup exhibits strong contact in the flat–head section and gentler contact in the ball–head section. Compared to a fully flat–head configuration, it reduces the overall contact intensity; compared to a fully ball–head configuration, it improves threshing efficiency. Thus, this configuration demonstrates the best performance among all structures in the single–factor experiment, providing a theoretical basis for structural optimization of the threshing device.

Figure 9b illustrates the effect of threshing element rotational speed (from 400 r/min to 800 r/min) on contact force with corn ears. As shown, the contact force spikes sharply at the beginning, because initially, it is difficult to detach the kernels from the cob, leading to a surge in contact force. Subsequently, the force fluctuates within a range – this is because once some kernels around a corn ear are detached, the threshing load required to remove the remaining kernels decreases. Therefore, as the threshing element acts on different parts of the ear, the contact force exhibits fluctuations and a general downward trend. It can also be seen from Figure 9b that the contact force increases with higher rotational speeds of the threshing element. Specifically, when the drum speed is 800 r/min, the average maximum contact force reaches 420.1 N, while at 400 r/min, it is only 274.4 N. This is because a higher drum speed results in a higher velocity of the threshing elements, thus increasing the impact load on the corn ears; conversely, lower speeds reduce the impact load. In addition, under the condition of 400 r/min, an abnormally high contact force is observed in Region A. This suggests that when the speed is too low, the flexible threshing element is unable to immediately separate the kernels from the cob. Only when the element deforms to its limit, or even transitions to a rigid state, can separation occur, resulting in a sustained high contact force over time. This also indicates that excessively low drum speeds are not suitable for flexible threshing. According to the literature, if the contact force on corn kernels during threshing exceeds 400 N, the risk of kernel breakage increases significantly *(Dandan et al., 2021)*. Considering both breakage rate and threshing efficiency, rotational speeds of 500 r/min, 600 r/min, and 700 r/min are identified as optimal.

Figure 9c presents the simulation results for threshing elements of different masses. As the mass of the threshing element increases, the impact force generated during contact with the corn kernels increases significantly. A comprehensive analysis shows that although increasing the element mass helps enhance the threshing intensity, an excessively high mass substantially increases the contact force, which may lead to a higher kernel breakage rate. Conversely, a mass that is too low results in insufficient threshing capacity, thus increasing grain loss. Compared to other masses, threshing elements weighing 230 g, 200 g, and 170 g demonstrate a better balance between achieving higher threshing efficiency and maintaining a lower breakage probability.

Based on the results of the single–factor simulation experiments, the selected range of rotational speed parameters is set to 500 r/min, 600 r/min, and 700 r/min, while the selected range of mass parameters is 230 g, 200 g, and 170 g. According to the simulation data on the effect of the threshing element structural form on threshing performance, the combination configuration outperforms the other two single-element configurations. This provides a theoretical basis for further validation through bench-scale experiments.

Orthogonal Experiment and Verification

To determine the optimal combination of operating parameters, a three-factor, three-level Box-Behnken response surface design was developed based on the results of single-factor experiments. Within the optimized parameter ranges identified through simulation testing, rotational speeds of 500 r/min, 600 r/min, and 700 r/min, and threshing component masses of 170 g, 200 g, and 230 g were selected for the trials. The coded levels of the experimental factors are shown in Table 5.

Table 5

Coding table of test factors

Level	Factor		
	Rotational Speed X_1(r/min)	Quality X_2 (g)	Component Structure X_3
-1	500	170	ball-head
0	600	200	Combination type
1	700	230	flat-head

The experimental design and results are shown in Table 6, where X1, X2 and X3, represent the coded values of the experimental rotational speed, threshing element mass, and threshing component combination respectively, Y1 and Y2 respectively represent the kernel breakage rate and the unthreshed rate.

Table 6

Design and results of simulation test

Test number	Rotational Speed X_1(r/min)	Quality X_2(g)	Component Structure X_3	Y1/%	Y2/%
1	-1	1	0	5.65	1.89
2	0	0	0	3.88	0.88
3	0	-1	-1	4.58	2.14
4	-1	-1	0	4.72	1.95
5	0	0	0	4.05	1.04
6	-1	0	1	4.31	1.81
7	-1	0	-1	4.42	2.18
8	1	0	-1	4.53	1.68
9	1	0	1	5.22	0.41
10	0	0	0	3.95	0.96
11	1	-1	0	5.83	2.01
12	0	1	1	5.39	0.82
13	0	0	0	4.05	0.75
14	0	1	-1	5.42	1.14
15	0	0	0	3.95	0.84
16	0	-1	1	4.90	1.41
17	1	1	0	5.94	0.33

Analysis of Experimental Results

To analyze the significance of rotational speed, threshing element mass, and threshing component combination on each evaluation index, analysis of variance (ANOVA) and significance testing were performed on the kernel breakage rate and threshing loss rate using Design-Expert software. The results are presented in Table 7.

Table 7

Analysis of airflow velocity in front of screen

Analysis of variance

Source	df	Grain breakage rate Y1		Unthreshed grain rate Y2	
		F Value	P-value	F Value	P-value
Model	9	113.1	< 0.0001	39.73	< 0.0001
X1	1	78.39	< 0.0001**	87.31	< 0.0001**
X2	1	81.37	< 0.0001**	83.76	< 0.0001**
X3	1	10.61	0.0139*	54.66	0.0002**
X1 X2	1	18.08	0.0038	39.65	0.0004
X1X3	1	22.32	0.0021	12.24	0.01
X2 X3	1	7.38	0.0299	2.54	0.1551
X12	1	179.01	< 0.0001	40.05	0.0004
X22	1	566.52	< 0.0001	16.45	0.0048
X32	1	4.97	0.061	13.37	0.0081
Residual	7				
Lack of fit	3	1.78	0.2908	1.79	0.289
Pure error	4				
Total error	16				

Note: *significant (P<0.05), **very significant (P<0.01)

Based on the data in Tables 7, the rotational speed, threshing component mass, and threshing component combination form exhibit varying degrees of influence on the grain breakage rate and threshing loss rate. All three parameters are significant factors affecting both the breakage rate and the threshing loss rate of corn kernels. Among them, the primary to secondary factors influencing the breakage rate (Y1), in descending order of importance, are: threshing component mass > rotational speed > component combination form. For the threshing loss rate (Y2), the order of influence is: rotational speed > threshing component mass > component combination form.

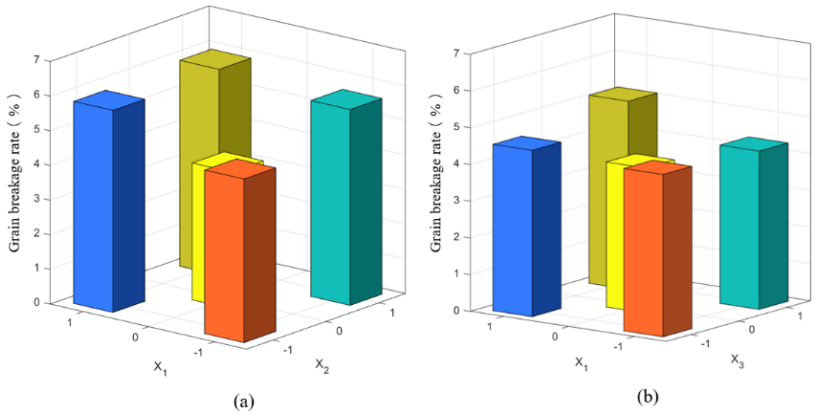

Fig. 10 - Response Surface Diagram of Interaction Factors for Kernel Breakage Rate

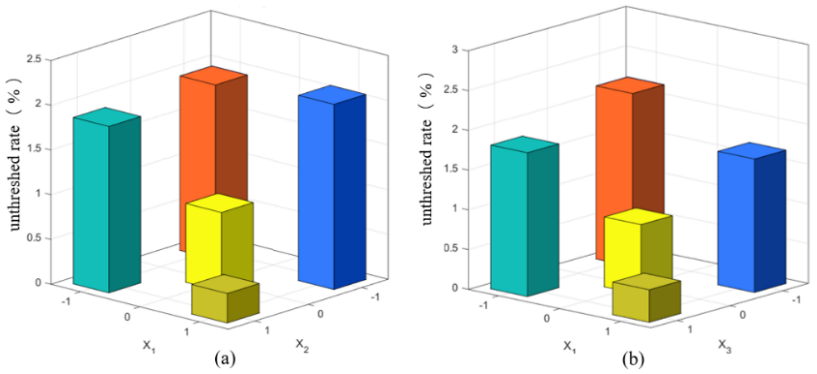

Fig. 11 - Response Surface Diagram of Interaction Factors for Unthreshed Rate

As shown in Figure 10a, the kernel breakage rate initially decreases and then increases with the rise in both the rotational speed and mass of the threshing element. The highest breakage rate occurs when both speed and mass are at high levels, while the lowest breakage rate is observed when these parameters are at moderate levels. Notably, a higher breakage rate is also observed under low–speed and low–mass conditions. This trend can be attributed to the fact that increasing the rotational speed raises the linear velocity of the threshing element, thereby increasing the impact kinetic energy. Simultaneously, an increase in mass amplifies the inertial force, resulting in greater instantaneous impact loads on the kernels. When both speed and mass are elevated, the combined impact intensity significantly increases, making the kernels more susceptible to breakage. Conversely, at low speed and mass, the flexible threshing effect is reduced, leading to higher stress on the kernels and thus greater breakage.

Figure 10b shows that under constant mass conditions, the influence of the threshing element's structural configuration on kernel breakage rate becomes more pronounced with increasing rotational speed. As the structure transitions from spherical to composite and cylindrical forms, the breakage rate increases accordingly. The cylindrical threshing element exhibits consistently higher breakage rates across all rotational speeds. In general, the higher the speed, the greater the structural configuration's impact on kernel breakage rate.

As shown in Figure 11a, the unthreshed rate decreases with increasing threshing element rotational speed and mass, indicating a negative correlation between these two factors and the unthreshed rate. The underlying reason is that a higher rotational speed increases the number of contacts between the threshing element and the corn ear, facilitating the detachment of kernels. Likewise, an increase in the element' s mass enhances the impact force, thereby improving threshing completeness.

In Figure 11b, under the same mass condition (200 g), notable differences in threshing performance are observed among different structural configurations of the threshing elements. The cylindrical structure results in the lowest unthreshed rate, suggesting that its smaller contact surface generates a more concentrated impact force, significantly improving threshing efficiency. Conversely, the spherical structure yields the highest unthreshed rate, likely due to its larger contact area, which weakens the impact and leaves some kernels unthreshed. At lower rotational speeds, the structural configuration of the threshing element has a greater effect on the unthreshed rate.

The optimal combination of parameters for this threshing device is: rotational speed of 600 r/min, threshing element mass of 200 g, and a combination-type configuration.

CONCLUSIONS

This study investigates a novel flexible corn threshing technology and develops an experimental bench in which threshing elements are hinged to the threshing rods. A series of single–factor simulations and multifactor orthogonal experiments were conducted, leading to the following conclusions:

By analyzing the impact loads during the operation of both rigid and flexible structures, the superiority of the single–point hinged flexible configuration over the rigid one was demonstrated. A contact force model between the flexible threshing element and the corn ear was established, and key operational parameters were identified.

Using the DEM–MBD coupled simulation method, the effects of threshing element mass, rotational speed, and structural configuration on contact force and adhesive bond failure between kernels and cobs were systematically analyzed. The results provided the basis for determining the test parameter range for bench-scale experiments.

Response Surface Methodology (RSM) optimization experiments revealed that the primary factors affecting the kernel breakage rate are: threshing element mass > rotational speed > structural configuration; while for the unthreshed rate, the order of influence is: rotational speed > mass > configuration. Considering both kernel breakage and unthreshed rate, the optimal working parameters were identified as a threshing element mass of 200 g, rotational speed of 600 r/min, and a combination-type configuration. Under these conditions, the kernel breakage rate was 3.95%, and the unthreshed rate was 0.88%.

The threshing principle and structural approach proposed in this study effectively mitigate the high breakage rate caused by traditional rigid-impact methods. This research provides a feasible solution for efficient and low-damage direct harvesting of corn kernels and offers valuable insights for the development and engineering application of flexible threshing devices.

ACKNOWLEDGEMENT

This research was funded by the National Key R&D Program of China, grant 569 number 2021YFD2000502, and the Modern Agricultural Industrial System of 570 Shandong Province, grant number SDAIT-02-12.

REFERENCES

[1] Dandan H., Yang Z., Junshan N., Qiqiang L., Lin C., Qi C., Lihua Z. (2024). DEM model acquisition of the corn ear with bonded particle model and its simulated parameters calibration. *Granular Matter*, 26(2), 54.

[2] Duane L., Harry H., Ted H. (1972). Corn kernel damage due to high velocity impact. *Transactions of the ASAE*, 12(1), 330–331.

[3] Horabik J., Beczek M., Mazur R., Parafiniuk P., Ryżak M., Molenda M. (2017). Determination of the restitution coefficient of seeds and coefficients of visco-elastic Hertz contact models for DEM simulations. *Biosystems Engineering*, 161, 106–119.

[4] Jiale Z., Hainan Z., Han T., Xiaogeng W., Yajun Y. (2023). Bionic threshing component optimized based on MBD-DEM coupling simulation significantly improves corn kernel harvesting rate. *Computers and Electronics in Agriculture*, 212, 10672.

[5] Jun F., Zhi C., Lujia H., Luquan R. (2018). Review of grain threshing theory and technology. *International Journal of Agricultural and Biological Engineering*, 11(3), 12–20.

[6] Kiniulis V., Steponavičius D., Kemzūraitė A., Andriušis A., Juknevičius D. (2018). Dynamic indicators of a corn ear threshing process influenced by the threshing-separation unit load. *Mechanics*, 24(4), 412–421.

[7] Lin N., Zehao Z., Haoran Y., Jie M., Qinghao H., Yanan W., Duanyang G. (2024). Design and Experiment of Flexible Threshing Device with Variable Stiffness for Corn. *Agriculture*, 14(6), 836.
[8] Meizhou C., Guangfei X., Chuansu W., Peisong D., Yinping Z., Guodong N. (2020). Design and experiment of roller-type combined longitudinal axial flow flexible threshing and separating device for corn. *Transactions of the Chinese Society for Agricultural Machinery*, 51(10), 123–131.
[9] Mircea C., Nenciu F., Vlăduț V., Voicu Gh., Găgeanu I., Cujbescu D. (2020). Increasing the performance of cylindrical separators for cereal cleaning, by using an inner helical coil. *INMATEH – Agricultural Engineering*, 62(3), 249–258.
[10] Mousaviraad M., Tekeste M. (2024). Systematic calibration and validation approach for Discrete Element Method (DEM) modeling of corn under varying moisture contents (MC). *Journal of the ASABE*, 67(2), 259–274.
[11] Nenciu F., Mircea C., Vlăduţ V., Belc N., Berca L. (2021). Evaluation of wheat seed separation performances for new design of rotating cylindrical sieve, equipped with customizable homogenization coil, *20th International Scientific Conference Engineering for Rural Development*, vol. 20, pp. 1478-148, Jelgava, Latvia.
[12] Tang Q., Jiang L., Yu W., Wu J., Wang G. (2024). Design and experiment of high moisture corn threshing device with low damage. *INMATEH - Agricultural Engineering*, 74(3), 172–183.
[13] Vlădut N.-V., Biris S.St., Cârdei P., Găgeanu I., Cujbescu D., Ungureanu N., Popa L.-D., Perişoară L., Matei G., Teliban G.-C. (2022). Contributions to the mathematical modeling of the threshing and separation process in an axial flow combine. *Agriculture,* 12(10), 1520.
[14] Vlădut N.-V., Ungureanu N., Biris S.St., Voicea I., Nenciu F., Găgeanu I., Cujbescu D., Popa L.-D., Boruz S., Matei G., Ekielski A., Teliban G.C. (2023). Research on the identification of some optimal threshing şi separation regimes in the axial flow apparatus. *Agriculture,* 13(4), 838.
[15] Xiaoyu L., Yuefeng D., Lei L., Enrong M., Fan Y., Jun F., Liang Z. (2022). Research on the constitutive model of low-damage corn threshing based on DEM. *Computers and Electronics in Agriculture*, 194, 10672.
[16] Xiaoyu L., Yuefeng D., Jinglin G., Enrong M. (2020). Design, simulation, and test of a new threshing cylinder for high moisture content corn. *Applied Sciences*, 10(14).
[17] Xin Ping L. (2013). Study on relationship of feeding form and threshing-cleaning rate of corn ears. *Advanced Materials Research*, 753, 1462–1466.
[18] Yajun Y., Liangshan L., Jiale Z., Xiangeng W., Jun F. (2021). Optimal design and simulation analysis of spike tooth threshing component based on DEM. *Processes*, 9(7), 1163.
[19] Yuan S., Hao L., Yang X., Tao C., Zhe Q., Dongxing Z. (2018). Optimization and experiment of spike-tooth elements of axial flow corn threshing device (轴流式玉米脱粒装置钉齿元件优化与试验). *Transactions of the Chinese Society for Agricultural Machinery*, 49(S1), 258–265.
[20] Zhanbin, W., Zhenwei, W., Yinping, Z., Wenxi, Y., Yanjie, C., Chengqiang, L. (2020). Design and test of longitudinal axial flexible hammer-claw corn thresher (纵轴流柔性锤爪式玉米脱粒装置设计与试验). *Transactions of the Chinese Society for Agricultural Machinery*, 51(S2), 109–117.
[21] Zhe Q., Dongxing Z., Li Y., Tianliang Z., Zhendong W.,Tao C. (2018). Experiment on feed rate and cylinder speed of longitudinal axial flow threshing and separating device for maize (纵轴流玉米脱粒分离装置喂入量与滚筒转速试验). T*ransactions of the Chinese Society for Agricultural Machinery*, 49(2), 58–65.
[22] Zhenjie Q., Chengqian J., Dingguo, Z. (2017). Multiple frictional impact dynamics of threshing process between flexible tooth and grain kernel. *Computers and Electronics in Agricultur*e, 141, 276–285.